Journal of Materials Chemistry A

Accepted Manuscript

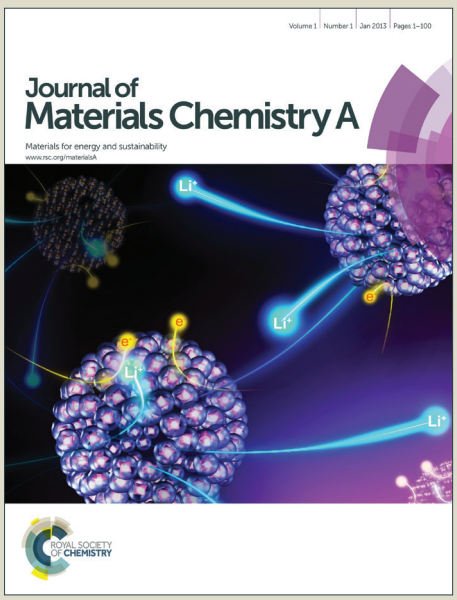

ROYAL SOCIETY OF CHEMISTRY

www.rsc.org/materialsA

Journal Name

RSCPublishing

ARTICLE

Generation of bimodal porosity via self-extra porogenes in nanoporous carbons for supercapacitor application

Cite this: DOI: 10.1039/x0xx00000x

Received 00th January 2012,
Accepted 00th January 2012

DOI: 10.1039/x0xx00000x

www.rsc.org/

Guangli Yu,[a] Xiaoqin Zou,*[a] Aifei Wang,[a] Jian Sun,[b] and Guangshan Zhu*[a]

In the present study, a facile strategy has been proposed for generating bimodal porosity in porous carbons, by using sacrificed metal organic framework (ZIF-8) as the precursor and additional silica colloids as extra porogenes via their further self-assembly. The details in the formation of hierarchical structures are studied by time-dependent XRD and TEM characterizations. As-synthesized hierarchical porous carbons possess micropores (1.0 nm) and mesopores (3~20 nm), which are verified by TEM and N_2-sorption measurements. The specific information on carbon structures is supplied by XRD and Raman data. The electrochemical properties have been briefly investigated by cyclic voltammetry and impedance spectroscopy. A highest capacitance of 181 F g^{-1} and lowest resistance of 0.21 Ω cm^2 are obtained between a series of ZIF-8 derivative carbons, both of which along with high electro-stability endow a promising application of these nanoporous carbons in supercapacitors.

Introduction

With increasing scarcity of energy resources, tremendous attention has been attracted to the development of energy storage devices or systems for capturing any possible energy to ensure their long-last uses. Among many energy-storage systems, supercapacitors or electric double-layer capacitors (EDLCs) [1-2] as an appealing representative are catching up our eyes owing to their high efficiency, ultralong cycle life and greenness. Since the electrode material plays a prime role in a supercapacitor, a variety of materials have been investigated for making electrodes.[3-7] Porous carbon with diversified micro- textures has been widely accepted to be the potential candidate for electrode materials mainly due to their lightweight properties, excellent chemical inertness, large specific surface area (SSA), and high conductivity etc.[8-11] Although great efforts have been made, there are still some hurdles to be overcome, for example, to construct an excellent supercapacitor with high energy as well as power density. In this regard, we can resort to design better porous carbon materials with superior properties in terms of high porosity, controllable pore size, and tunable interconnected pore structure.[8, 12] Porosity is the fundamental characteristic of nanoporous carbons. High porosity means a large number of voids in carbons, providing large space for guest accommodation, especially for electrons. Meanwhile, pore size is another important parameter, because unique interaction between molecules or ions within the nanospaces network is due to size selection effect. Additionally, the pore structure plays a crucial role for guests' mobility and space accessibility, which has to be taken into account during the designed synthesis of nanoporous carbons. Therefore, the creation of pores with precise control over pore size and shape is of great interests for scientists and engineers.

Up to now, several synthetic methods to prepare porous carbons have been established, including laser ablation,[13] electrical arc,[14] chemical vapor decomposition (CVD),[15] and chemical or physical activation[16] as well as template carbonization.[17-18] In the former several routine routes, pores in the size range of nano to micrometers can be created inside carbon skeletons. The resultant porous carbons possess high surface area; however, their structures are disordered and random pores with broad pore size distributions, thereby losing their advantage in molecular recognition. In the latter template route, the creation of micro- or mesoporous carbons involves selecting appropriate carbon gels and templates followed by further carbonization. The typical examples include hard or soft-template methods by impregnation or chemical deposition of carbon sources within ordered porous solids (e.g. zeolites, mesoporous silica)[18-20] or self-assembly of carbon gels by polymerizing around surfactants.[21-23] Although ordered porous carbons can be prepared via this method, single-modal pores (either micro or mesopores) are obtained in one specific carbon entity. In addition, only a few stable carbon gels have been found to be suitable; and the preparation process is quite complicated and unfavorable for large-scale production of porous carbons.

Very recently, microporous carbons can be derived from metal organic frameworks (MOFs),[24] evidenced by several examples (MOF-5, Al-PCP, ZIF-8).[25-28] MOFs are considered as alternative precursors for constructing nanoporous carbons due to their periodic structures, adjustable pores, high specific surface areas and abundant carbon atoms in skeletons, which can broaden the library of porous carbons with novel structures and functions.[29] The preparation of porous carbons with both micro and mesopores in the frameworks is still a big challenge using MOFs as precursors, because multi-modal porosity can bring benefits in high capacitance and low transport resistance. Based on the considerations above, herein, our interests rely on proposing a new and facile strategy to simultaneously generate micro-meso porosities in carbons from cheap precursors, exemplified by loading commercially available silica nanoparticles inside the zeolite imidazolate framework crystals (ZIFs, a subclass of MOFs). Typically, ZIF-8 [$Zn(MeIM)_2$, MeIM=2-methylimidazolate][30] is selected as the host material to introduce microporosity because it possesses quite thermal stability to ensure complete carbonization before ligand decomposition (structure collapse), 3-D open framework, large surface area and high carbon content. Additionally, small silica particles with size falling in the mesopore range (2-50 nm, IUPAC) are introduced to generate supplementary pores into ZIF-8 entities by removing these porogenes. Further, as-prepared nanoporous carbons are explored in the application of electrode materials as supercapacitors. High capacitance of 187 F g^{-1} and low electrochemical impedance of 0.21Ω cm^2 are obtained, benefited from well-balanced micro-meso porosities.

Experimental

Materials and methods

Zinc nitrate hexahydrate ($Zn(NO_3)_2 \cdot 6H_2O$, Sinopharm Chemical Reagent Shanghai Co., Ltd., China, AR), 2-methylimidazole (MeIM, Chengdu Kelon Chemical Reagent Factory, AR), colloidal silica (Ludox AS-30, Sigma-Aldrich, 30 wt.% suspensions in water), n-butylamine ($C_4H_{11}N$, Tianjin Fuchen Chemical Reagent Factory, AR), fumed silica AS-200 (SiO_2, Shenyang Chemical Co., Ltd., China, 99%), anhydrous methanol (CH_3OH, Tianjin Guangfu Chemical Research Institute, GR), ethanol and hydrofluoric acid (40% HF, Xilong Chemical Co., Ltd., AR) were used as received without any further purification.

The powder X-ray diffraction (PXRD) measurements were performed by using Riguku D/MAX2550 diffractometer with Cu-Kα radiation (50 kV, 200 mA, λ = 1.5418Å) and a scanning step of 0.02º. The morphologies and structures of all samples were obtained by transmission electron microscopy (TEM, JEOL JSM-3010). Particle size distributions of silica were examined by means of dynamic light scattering (DLS) analysis using a Malvern Zetasizer-Nano instrument. Raman spectra were recorded on a Micro-Raman system from Renishaw/UK using an Ar ion laser with an excitation wavelength of 532 nm. The silica amounts in ZIF-8 crystals were determined by XPS on a Scienta ESCA 200 spectrometer. Thermogravimetric analyses of the samples were performed on a Netzch Sta 449c thermal analyzer with a heating rate of 10 K min^{-1} under air atmosphere. Nitrogen adsorption and desorption experiments were carried out at 77 K on an Autosorb iQ2 adsorptometer, Quantachrome Instrument. Prior to the tests, the samples were degassed at 423 K overnight under vacuum. Specific surface areas were calculated by using the Brunauer-Emmett-Teller (BET) equation; and the pore volumes and pore size distributions were determined by applying t-plot and BJH, and the non-local density functional theory (NL-DFT) methods respectively.

Synthesis of silica/ZIF-8 nanocrystals

Nanocrystals of neat ZIF-8 were prepared according to the previous report with a slight modification.[30] Typically, solution A was prepared by dissolving 0.147 g $Zn(NO_3)_2 \cdot 6H_2O$ in 10 mL CH_3OH, meanwhile 0.081 g 2-methylimidazole and 0.195 mL n-butylamine were dispersed in another 10 mL CH_3OH to form solution B. And then, both solutions were mixed together under stirring for 12 hours at room temperature. The yielded ZIF-8 powder was purified by repetitive centrifugations (10000 rpm, 3 minutes) using CH_3OH as the solvent with subsequent drying in air.

For the preparation of silica/ZIF-8 crystals (L-ZIF-8 and F-ZIF-8), solution C (total 10 mL) instead of solution B was prepared by separately dissolving 0.081 g 2-methylimidazole and 0.195 mL n-butylamine in 5 mL CH_3OH, and 1 g fumed silica aqueous solution (0.3 g fumed silica in 0.7 g water) in another 5 mL CH_3OH. Solution C was homogeneously mixed with 10 mL solution A containing zinc source (F-ZIF-8). The similar procedure was also employed for the synthesis of L-ZIF-8 by simply substituting fumed silica with 1 g Ludox solution (30 wt. %, the silica mass of 0.3 g is the same as in F-ZIF-8). The following procedures including room-temperature crystallization, powder purification and sample drying were exactly the same as stated above for that of ZIF-8.

Preparation of porous carbons

As-prepared silica/ZIF-8 or ZIF-8 samples were introduced inside a quartz boat, which was placed at the center of a quartz tube with both ends connected to argon gas. The tubular furnace was heated up at 1073 K for 5 hours with a ramp of 1 K min^{-1} under continuous argon flow of 50 mL min^{-1}. The carbonized products were further treated thoroughly with HF aqueous solution (10 wt. %) to remove residual inorganic matters and washed extensively with deionized water until neutral pH. The completion of silica removal was confirmed by the disappearance of Si (2p) associated peaks (103 eV) in XPS spectra of Fig. S1 (X-ray photoelectron spectroscopy). The resultant carbons were dried at 373 K overnight.

Electrochemical measurements

Electrochemical measurements were performed on a Zennium electrochemical workstation (Zahner, Germany) in a standard three-electrode system at room temperature. A platinum gauze

electrode and a saturated calomel electrode (SCE) were served as the counter and reference electrodes in 6 M KOH electrolytes, respectively. All the working electrodes were fabricated by firstly mixing 75 wt. % powdered active carbon materials (C-ZIF-8, LC-ZIF-8, FC-ZIF-8), 15 wt. % acetylene black and 10 wt. % polytetrafluoroethylene (PTFE) dispersed in ethanol solvent to form slurry, and then depositing onto nickel foam with an area of effective area around 1.0 cm^2 and a film thickness of 0.14-0.16 mm (the apparent electrode density is about 0.56 g cm^{-3}). The foam was dried overnight at room temperature and then pressed under 25 MPa as a working electrode. Cyclic voltammetry (CV) and electrochemical impedance spectroscopy (EIS) were used for the evaluation of electrochemical performances of the electrode materials.

Results and discussion

XRD studies

The crystalline structures of fresh-prepared MOFs (labeled as ZIF-8, L-ZIF-8, F-ZIF-8 for neat ZIF-8, ludox-ZIF-8, fumed silica-ZIF-8 samples) and their corresponding derivative carbon materials (labeled as C-ZIF-8, LC-ZIF-8, and FC-ZIF-8) were determined using powder X-ray diffraction (XRD). As depicted in Fig. 1a, hybrid materials of L-ZIF-8 and F-ZIF-8 exhibited similar diffraction patterns to that of neat ZIF-8, indicating both samples possess the same structure as ZIF-8 with high crystallinity and free of other impure crystalline phases. With a close look, small broad peaks are detected in 2θ of 20-25º in the patterns of L-ZIF-8 and F-ZIF-8 originating from amorphous silica. This point out small silica particles from ludox and fumed silica are incorporated in ZIF-8 crystals. Fig. 1b displays XRD patterns of carbon derivatives, which are obtained by the carbonization of as-synthesized ZIF-8 samples with subsequent silica removal using HF solution. Peaks centered at around 24.5º and 44º are ascribed to the diffractions of (002) and (100) planes of carbon (JCPDS 01-0640), respectively. The peak in presence at 44º also tells us that graphitization in some extent is taking place during the carbonization process.

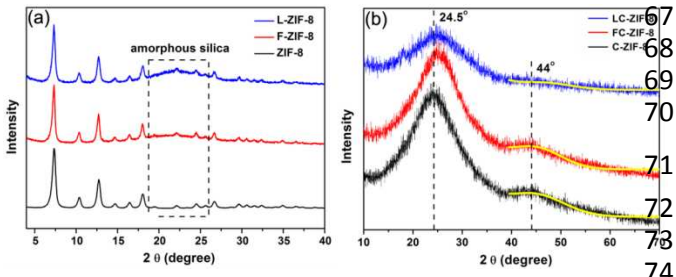

Fig. 1 XRD patterns of prepared ZIF-8 hybrids and the corresponding carbon materials.

Raman studies

Raman spectroscopy is generally used for probing local structures of graphitic carbon species. As shown in Fig. 2, two major bands are observed in all prepared carbons, assigning to the vibration modes of D and G bands.[31] By deconvolution of the two superimposed bands, about 25% graphitic carbons (calculated from G band areas) are present in the samples after carbonization, in couple with ~75% amorphous carbons.

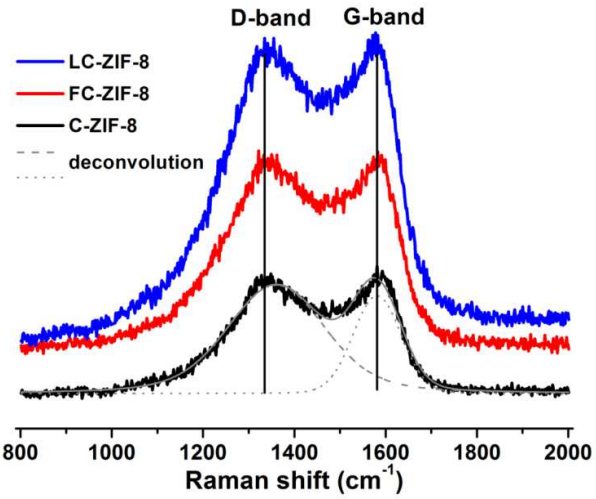

Fig. 2 Raman spectra of ZIF-8 derived carbons.

TEM studies

The morphologies of as-synthesized ZIF-8 hybrids and carbons are visualized by transmission electron microscopy (TEM). As seen in Fig. 3a, ZIF-8 crystals exhibit spherical shapes with an average size of 25 nm. Also, ZIF-8 hybrids have similar morphology to neat ZIF-8 (Fig. S2). The carbon particles (Fig. 3d) merge together after carbonization, which are different from the discrete ZIF-8 crystals (Fig. 3a). With zooming, many small voids of around 1.0 nm are visible in C-ZIF-8 particles (Fig. 3d), the size of which coincides with the cavity diameter of ZIF-8 crystals (1.1 nm).[30] For LC-ZIF-8 (Fig. 3e), besides the small pores, some large voids of about 2.7 nm are observed as well. These big pores are generated by removing silica colloids of 4 nm embedded in L-ZIF-8 crystals (Fig. 3b); and this size also matches well with the particle size distribution of colloidal silica in solution (Fig. S3). For FC-ZIF-8 (Fig. 3f), similar large voids of 14 nm are detected by TEM within carbon particles. The creation of defined big pores falling in mesopore scale (similar to the size of fumed silica, see Fig. S3) is benefited from the encapsulated silica in F-ZIF-8 crystals (Fig. 3c).

Porosity studies

The porosity and specific surface areas in all prepared samples are investigated in details by nitrogen adsorption measurements. Fig. 4 shows adsorption-desorption isotherms of C-ZIF-8, LC-ZIF-8 and FC-ZIF-8, typical for Type IV isotherms. A steep uptake at low relative pressures followed by a plateau is recorded, suggesting that many micropores exist in the carbons. To be noted, a distinct hysteresis at high relative pressures is also detected, shedding light on the occurrence of mesopores. The textural data including specific Brunauer-Emmett-Teller surface area (S_{BET}) and micropore-mesopore volumes are

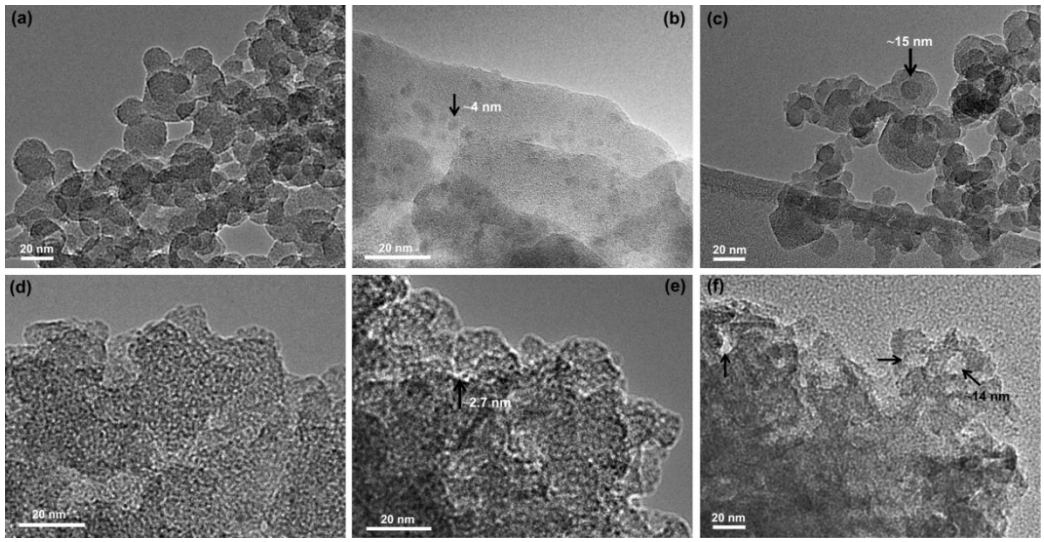

Fig. 3 Representative TEM images of prepared neat ZIF-8 (a), silica-ZIF-8 hybrids of L-ZIF-8 (b), F-ZIF-8 (c); and their corresponding carbon materials of C-ZIF-8 (d), LC-ZIF-8 (e), and FC-ZIF-8 (f).

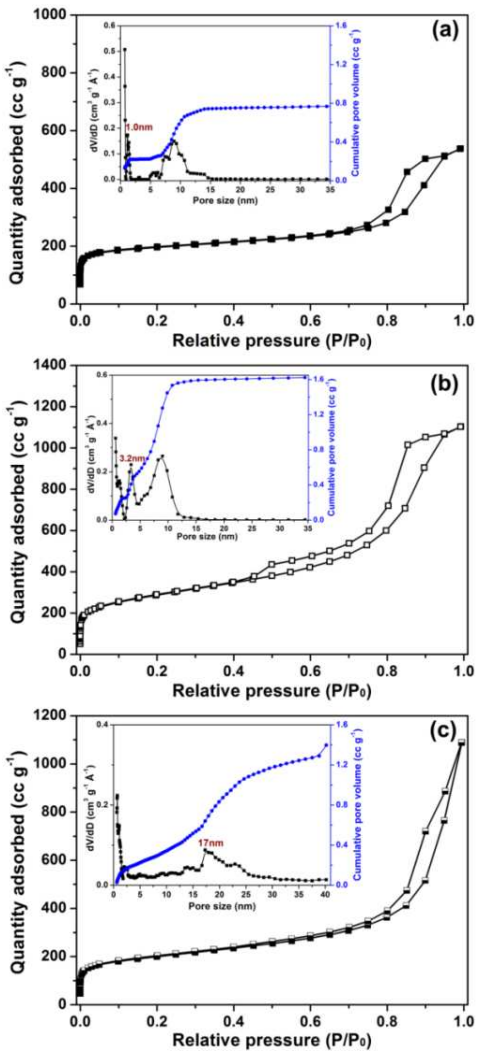

Fig. 4 N_2 adsorption isotherms and pore size distribution curves of C-ZIF-8 (a), LC-ZIF-8 (b) and FC-ZIF-8 carbons (c).

summarized in Table S1. It can be found that the obtained carbons are highly porous with surface areas above 700 $m^2 g^{-1}$; a largest surface area of 1026 $m^2 g^{-1}$ and pore volume of 1.71 $cm^3 g^{-1}$ is obtained for LC-ZIF-8, because of its three-fold pore structure of 1.0, 3.2 and 8.0 nm. The corresponding pore size distributions for all three samples are shown in insert pictures of Fig. 4. All samples exhibit almost identical micropore size of 1.0 nm. This expectation can be explained with the inherent micropores stemmed from the well-ordered cavities of ZIF-8 crystals, consistent with XRD and TEM results. Interestingly, the sizes of present mesopores vary differently from C-ZIF-8 to LC-ZIF-8 and FC-ZIF-8. Typically, the mesopore size is about 8 nm for C-ZIF-8, which is derived from self-aggregating effect of carbon nanoparticles. For LC-ZIF-8, in addition to large pores (8.0 nm), small mesopores around 3 nm are generated. The pore size is in good agreement with visible voids in the TEM image as displayed in Fig. 3e. For FC-ZIF-8, the mesopore size is shifted to a high value of 17 nm. This means these secondary pores are coming from the removal of colloidal silica with specific diameters, which are evidenced by their particle size distributions (Fig. S3). Additionally, the ratios between micropore and mesopore volumes can be tuned in a range of 0.1-0.4 by varying the amounts of extra silica colloids, which is exemplified by the ratio values of 0.1, 0.23 and 0.38 in LC-ZIF-8 sample with 0.015, 0.0075, 0.00375 g mL^{-1} silica in ZIF-8 precursors.

Formation mechanism

To briefly investigate the formation mechanism of hierarchical ZIF-based porous carbons, combined techniques of XRD and TEM are used to follow its process. Time-dependent XRD patterns are shown in Fig. 5. ZIF-8 undergoes a rapid crystallization and its crystallinity reaches almost 100% after 30 minutes (calculated from their respective XRD patterns in Fig. S4). As seen from the morphology changes in TEM images,

more discrete ZIF-8 particles with regular shapes are formed with a prolonged crystallization time. However, the crystallization of L-ZIF-8 is much slower than that of ZIF-8, and the full crystallinity can be gained after 360 minutes. Silica colloids and ZIF-8 crystals are merged together as seen from TEM pictures. These observations suggest that colloidal silica in ZIF-8 precursors largely inhibits the crystallization of ZIF-8 crystals, while this inhibition can assist the co-assembly of silica and ZIF-8 precursor into a hierarchical composite.

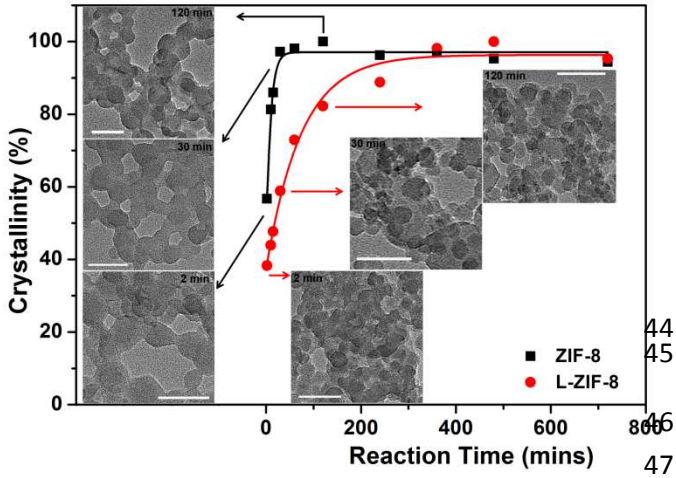

Fig. 5 The changes of relative ZIF-8 crystallinity in function of time (assuming the crystallinity of 100% for the samples after 12 h), and representative TEM pictures with corresponding time (2, 30, 120 minutes, scale bar of 50 nm).

For clear illustration, the process of pores formation is proposed in Scheme 1. ZIF-8 frameworks or sub-nano crystals are formed after immediately mixing their precursors of Zn and methylimidazole at room temperature. The crystallinity of ZIF-8 crystals is increasing with time, and micropores are spontaneously formed during the crystallization period. Meanwhile, colloidal silica is embedded in the precursor with subsequent incorporation inside or between aggregated crystals as crystallization progresses on (Scheme 1). Upon heating at high temperatures (>973 K), the ligands of 2-methylimidazolate start to be decomposed, immediately with the subsequent carbonization; leaving the internal voids of crystals intact (micropores). Due to self-aggregation, some big pores (mesopores) are formed between carbon particles during the carbonization stage. In an alternative way, new supplementary mesopores are yielded with a further removal of resided silica in the carbons. Based on the observations above, one can conclude that the micropores in porous carbons are inherited from the intrinsic ZIF-8 cavities; while mesopores are produced during self-assembly or extraction of extra silica porogenes.

Thermal stability

The thermal stability of porous carbons was evaluated by thermogravimetric analysis (TGA) in air. Fig. 6 shows the TG curves of C-ZIF-8, LC-ZIF-8 and FC-ZIF-8 samples respectively. The curves exhibit similar shapes, with a small weight loss of ~15 wt. % in the temperature of 25-120 °C which is attributed to the removal of adsorbed water. A big weight loss is observed from onset temperature around 500 °C, which corresponds to the combustion of carbons. These results confirm that obtained porous carbons are stable up to 500 °C.

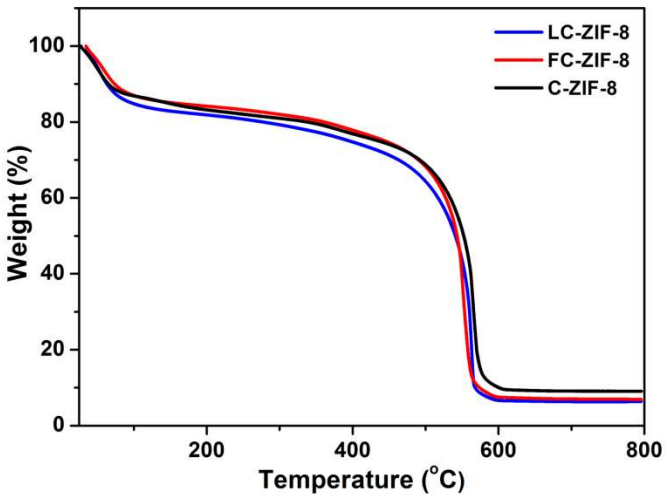

Fig. 6 TG curves of C-ZIF-8, LC-ZIF-8 and FC-ZIF-8 carbons

Electrochemical characteristics

It is widely accepted that hierarchical porous carbons can bring many benefits to the electrochemical properties of supercapacitors, including high capacitance and fast ions transport in the electrodes.[2,8] Motivated by the bimodal porosity of as-prepared porous carbons, electrochemical capacitive performances are studied, exemplified by cyclic voltammetry (CV) and electrochemical impedance spectroscopy (EIS) techniques. The CV profiles of porous carbons at various sweep rates from 5 to 100 mV s^{-1} are collected in Fig. 7. All samples exhibit relatively good rectangular curves at 5 mV s^{-1}, and retain quasi-rectangular shapes at high sweeping rates; demonstrating effective double charged layers of K^+ ions (0.66 nm)[32-33] are built along the pores of 1.0 nm, and thus resulting in high gravimetric capacitances. The specific capacitances of C-ZIF-8 to LC-ZIF-8 and FC-ZIF-8 are calculated to be 181, 175 and 164 F g^{-1} at a sweep rate of 5 mV s^{-1} respectively, the values of which coincide with a similar trend of their micropore volumes (0.23, 0.16, 0.15 cm^3 g^{-1} for C-ZIF-8, LC-ZIF-8, FC-ZIF-8; Table S1). Such finding points out micropores of 1.0 nm in obtained carbons play a crucial role in charge storage, while the introduction of silica slightly contribute to the capacitances. Meanwhile, the high capacitances guarantee these ZIF-8 derived carbons to be excellent electrode materials.

Besides, the resistance for ion transportation is another important parameter in carbon-based electrodes. In this respect, the impedance spectrum can be used to estimate the ion transport/diffusion ability within the pores. Fig. 8 provides Nyquist plots for all the carbon samples in frequencies between 10^5 Hz and 0.1 Hz at an open circuit voltage. Apparently, the impedance plots show an increasing trend with a nearly vertical

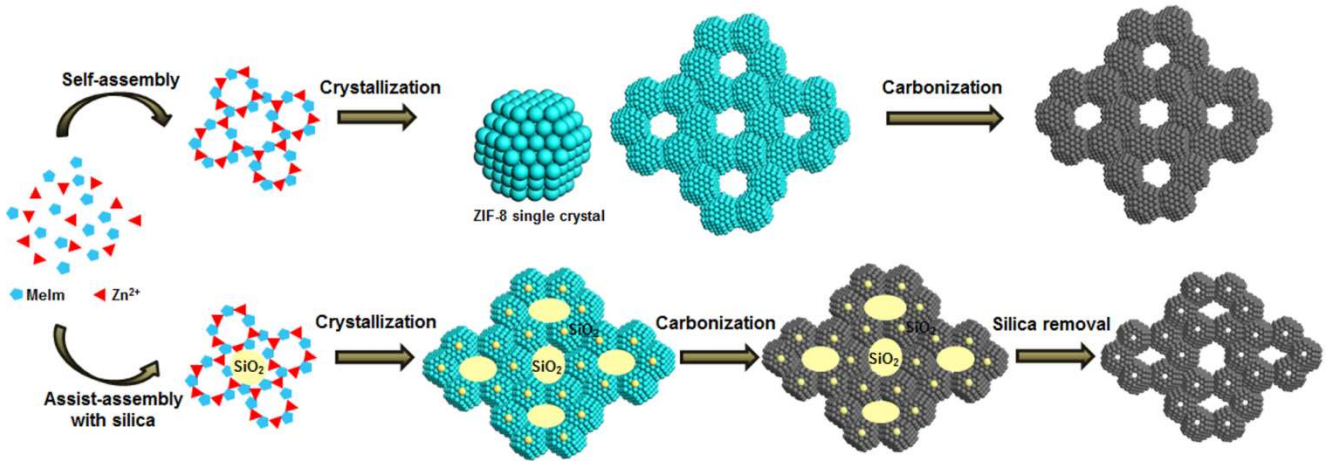

Scheme 1 Formation process of porous carbons with bimodal porosity via self and assisted assembly approaches

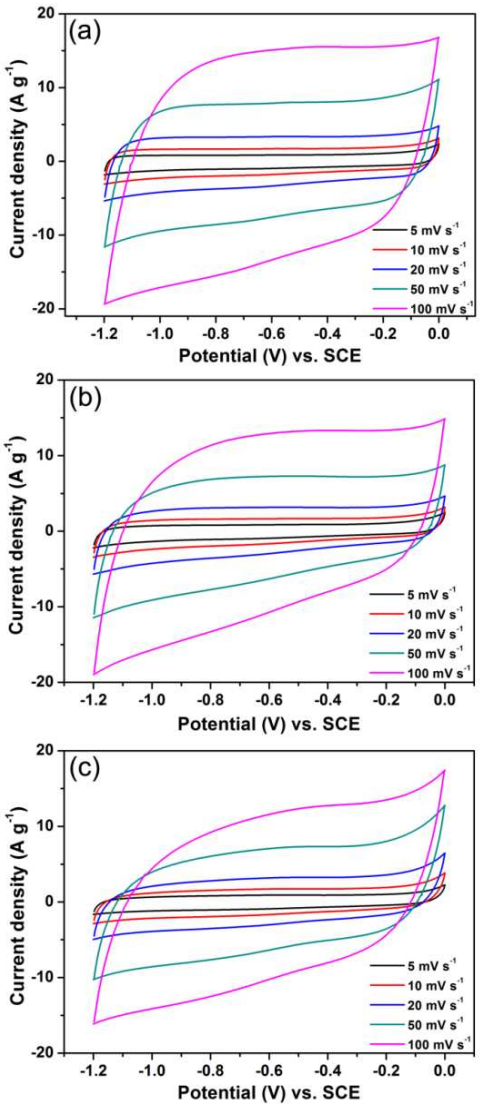

Fig. 7 CV curves of C-ZIF-8 (a), LC-ZIF-8 (b) and FC-ZIF-8 (c) at different scan rates.

line in the low frequency region, which indicates a good capacitive behavior, in accordance to CV results. The inserted sub-plot in Fig. 8b depicts the magnified impedance spectrum at the high frequency region. Obviously, equivalent series resistance (ESR) of LC-ZIF-8 and FC-ZIF-8 are 0.21 and 0.25 Ω cm^2 respectively, which is much lower than that of C-ZIF-8 (0.42 Ω cm^2). The lower resistance can be attributed to the existence of big pores, as proven by high mesopore volumes for LC-ZIF-8 and FC-ZIF-8 samples in Table S1.

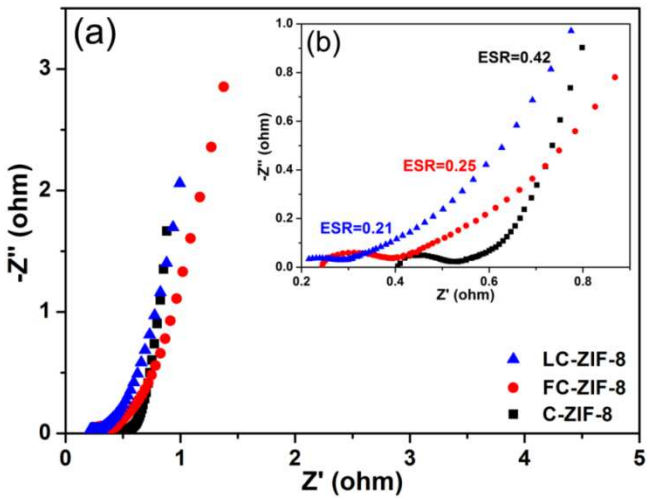

Fig. 8 Nyquist plots of obtained porous ZIF-8 derived carbons at different frequencies.

This observation gives us a sound proof that large pores provide highways for ions to access the pore surface, thus enhance the ion diffusion rate. Moreover, the partial graphitization makes some contributions to electrical conductivity. To support this hypothesis, three samples with varied extents of graphitization were prepared simply by changing the carbonization temperatures (i.e. 1073-1273 K); and their corresponding results are shown in Table S2. As shown in Table S2, the contents of graphitic carbons in C-ZIF-8 samples are increasing

(from 25.0% to 34.2%) with elevated carbonization temperatures, thereby decreasing the ESR values (from 0.42 to 0.28 Ω cm^2). On the basis of electrochemical results, it can be concluded that bimodal porosity in hierarchical porous carbons not only improves charge storage in small pores but also facilitates electrolyte ion diffusion via large-pore channels.

Electrochemical performances

To further evaluate the rate performances of these materials, films with ZIF-8 derived carbons were tested with different scan rates. Specific capacitances obtained at increasing scan rates are shown in Fig. 9a. When a low scan rate of 5 mV s^{-1} is applied to the electrodes, the specific capacitances of 181, 175, 164 F g^{-1} are obtained for C-ZIF-8, LC-ZIF-8 and FC-ZIF-8. When the scan rate is increased to 200 mV s^{-1}, the capacitances decay to 55%, 74% and 70% of their initial values. LC-ZIF-8 and FC-ZIF-8 retain larger capacitances than C-ZIF-8 at high scan rates; benefited from higher ion mobility in large mesopore volumes (Table S1).

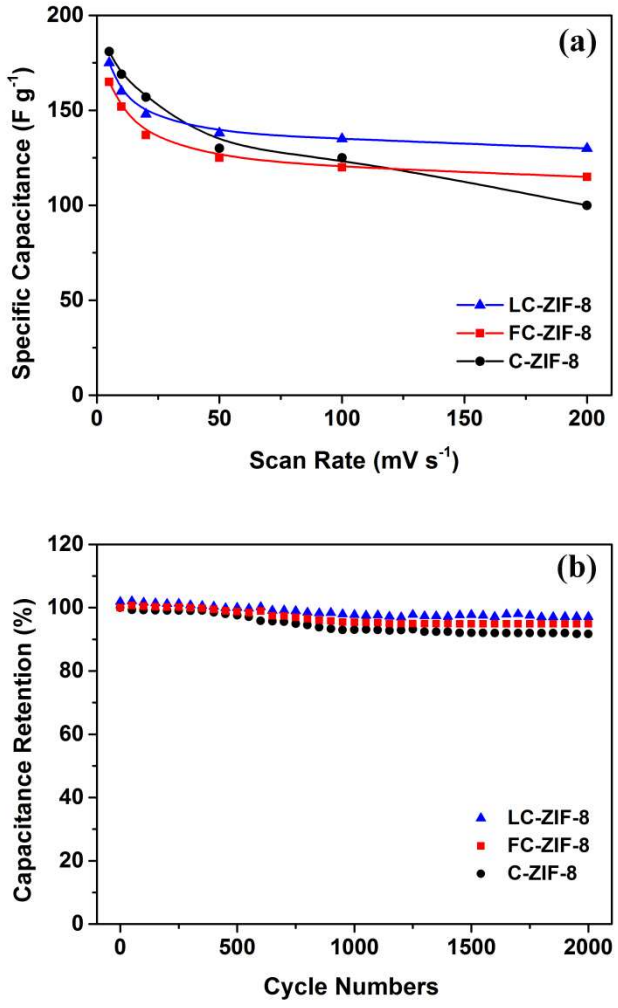

Fig. 9 Rate (a) and cycle (b) performances of C-ZIF-8, LC-ZIF-8 and FC-ZIF-8 electrodes at varied scan rates and a specific scan rate of 100 mV s^{-1}

The stability of these electrodes was also examined with repetitive tests. Fig. 9b shows times-resolved capacitances upon tests at 100 mV s^{-1}. As can be seen, all the samples exhibit good capacitance retention (92-97%) after 2000 consecutive cycles. Overall, ZIF-8 based porous carbons retain good rate performance and stability.

Conclusions

In conclusion, a new concept on how to introduce multi-porosity in porous carbons has been demonstrated, which is exemplified by a series of ZIF-8 derived carbon materials. We have found that the micropores around 1.0 nm are inherited from the intrinsic cavities of ZIF-8 crystals; while mesopores with pore size range of 3~20 nm are produced with an assistance of self-extra porogenes. The mesopore sizes as well as volumes can be simply varied by employing either ZIF-8 nanocrystals or added silica colloids with particular particle sizes and changing the introduced amounts, respectively. XRD and Raman results reveal that as-obtained porous carbons possess both graphitic and amorphous phases. The electrochemical properties on these three types of carbons are studied by measuring their cyclic voltammetry and impedance behaviors. The obtained results show that as-prepared porous carbons exhibit high capacitance and low resistance, which are benefited from high surface areas, high microporosity, and a large portion of mesoporosity in these carbons. Moreover, the electrodes made of these porous carbons exhibit good rate performance and stability. This new concept not only provides a strategy for the syntheses of hierarchical porous carbon materials from economic resources, but also offers a direction to design multi-porosity within carbons for improving their electrochemical performances as supercapacitor electrode materials.

Acknowledgements

We are grateful to the financial supports from National Basic Research Program of China (973 Program, grant no.2012CB821700), and NSFC project (grant nos. 21120102034, 20831002).

Notes and references

[a] State Key Laboratory of Inorganic Synthesis and Preparative Chemistry Jilin University, Changchun 130012, China E-mail: xiaoqinzou123@gmail.com; zhugs@jlu.edu.cn
[b] College of Chemistry, Jilin University, Changchun, 130023, P.R. China.

[1] P. Simon, Y. Gogotsi, *Acc. Chem. Res.* **2013**, *46,* 1094.
[2] H. Jiang, P. S. Lee, C. Z. Li, *Energy Environ. Sci.* **2013**, *6,* 41.
[3] P. Simon, Y. Gogotsi, *Nat. Mater.* **2008**, *7,* 845.
[4] C. G. Liu, Z. N. Yu, D. Neff, A. Zhamu, B. Z. Jang, *Nano Lett.* **2010**, *10*, 4863.
[5] L. Dai, D. W. Chang, J. B. Baek, W. Lu, *Small* **2012**, *8*, 1130.
[6] H. Nakanishi, B. A. Grzybowski, *J. Phys. Chem. Lett.* **2010**, *1*, 1428.
[7] Y. P. Zhai, Y. Q. Dou, D. Y. Zhao, P. F. Fulvio, R. T. Mayes, S. Dai, *Adv. Mater.* **2011**, *23*, 4828.
[8] L. L. Zhang, Y. Gu, X. S. Zhao, *J. Mater. Chem. A* **2013**, *1*, 9395.

[9] M. Rose, Y. Korenblit, E. Kockrick, L. Borchardt, M. Oschatz, S. Kaskel, G. Yushin, *Small* **2011**, *7*, 1108.
[10] W. Xing, C. C. Huang, S. P. Zhuo, X. Yuan, G. Q. Wang, D. Hulicova-jurcakova, Z. F. Yan, G. Q. Lu, *Carbon* **2009**, *47*, 1715.
[11] T. Y. Kim, G. Jung, S. Yoo, K. S. Suh, R. S. Ruoff, *ACS Nano*, **2013**, *7*, 6899.
[12] G. Feng, P. T. Cummings, *J. Phys. Chem. Lett*. **2011**, *2*, 2859.
[13] A. Thess, R. Lee, P. Nikolaev, H. J. Dai, P. Petit, J. Robert, C. H. Xu, Y. H. Lee, S. G. Kim, A. G. Rinzler, D. T. Colbert, G. E. Scuseria, D. Tománek, J. E. Fischer, R. E. Smalley, *Science* **1996**, *273,* 483.
[14] C. Journet, W. K. Maser, P. Bernier, A. Loiseau, M. L. D. L. Chapalle, S. Lefrant, P. Deniard, R. Lee, J. E. Fischer, *Nature* **1997**, *388*, 756.
[15] B. Zheng, C. G. Lu, A. Makarovski, G. Finkelstein, J. Liu, *Nano Lett.* **2002**, *2*, 895.
[16] H. Teng, S. C. Wang, *Carbon* **2000**, *38,* 817.
[17] A. H. Lu, F. Schüth, *Adv. Mater.* **2006**, *18*, 1793.
[18] T. Kyotani, T. Nagai, S. Inoue, A. Tomita, *Chem. Mater*. **1997**, *9,* 609.
[19] Z. X. Ma, T. Kyotani, Z. Liu, O. Terasaki, A. Tomita, *Chem. Mater.* **2001**, *13,* 4413.
[20] S. Jun, S. H. Joo, R. Ryoo, M. Kruk, M. Jaroniec, Z. Liu, T. Ohsuna, O. Terasaki, *J. Am. Chem. Soc*. **2000**, *122*, 10712.
[21] J. Wei, D. D. Zhou, Z. K. Sun, Y. H. Deng, Y. Y. Xia, D. Y. Zhao, *Adv. Funct. Mater*. **2013**, *23*, 2322.
[22] M. J. Zhong, E. K. Kim, J. P. McGann, S. E. Chun, J. F. Whitacre, M. Jaroniec, K. Matyjaszewski, T. Kowalewski, *J. Am. Chem. Soc*. **2012**, *134*, 14846.
[23] Z. A. Qiao, B. K. Guo, A. J. Binder, J. H. Chen, G. M. Veith, S. Dai, *Nano Lett*. **2013**, *13*, 207.
[24] W. Chaikittisilp, K. Ariga, Y. Yamauchi, *J. Mater. Chem. A* **2013**, *1*, 14.
[25] K. Xi, S. Cao, X. Y. Peng, C. Ducati, R. V. Kumar, A. K. Cheetham, *Chem. Commun*. **2013**, *49*, 2192.
[26] L. Radhakrishnan, J. Reboul, S. Furukawa, P. Srinivasu, S. Kitagawa, Y. Yamauchi, *Chem. Mater*. **2011**, *23*, 1225.
[27] B. Liu, H. Shioyama, T. Akita, Q. Xu, *J. Am. Chem. Soc*. **2008**, *130*, 5390.
[28] H. L. Jiang, B. Liu, Y. Q. Lan, K. Kuratani, T. Akita, H. Shioyama, F. Q. Zong, Q. Xu, *J. Am. Chem. Soc.* **2011**, *133*, 11854.
[29] H. Furukawa, K. E. Cordova, M. O′Keeffe, O. M. Yaghi, *Science* **2013**, *341*, 974.
[30] K. S. Park, Z. Ni, A. P. Côté, J. Y. Choi, R. Huang, F. J. Uribe-Romo, H. K. Chae, M. O′Keeffe, O. M. Yaghi, *Proc. Natl. Acad. Sci*. **2006**, *103,* 10186.
[31] Z. W. Xu, Z. Li, C. M. B. Holt, X. H. Tan, H. L. Wang, B. S. Amirkhiz, T. Stephenson, D. Mitlin, *J. Phys. Chem. Lett*. **2012**, *3*, 2928.
[32] X. Q. Zou, G. S. Zhu, H. L. Guo, X. F. Jing, D. Xu, S. L. Qiu, *Microporous Mesoporous Mater*. **2009**, *124,* 70.
[33] M. Kazemimoghadam, T. Mohammadi, *Desalination* **2007**, *206*, 547.

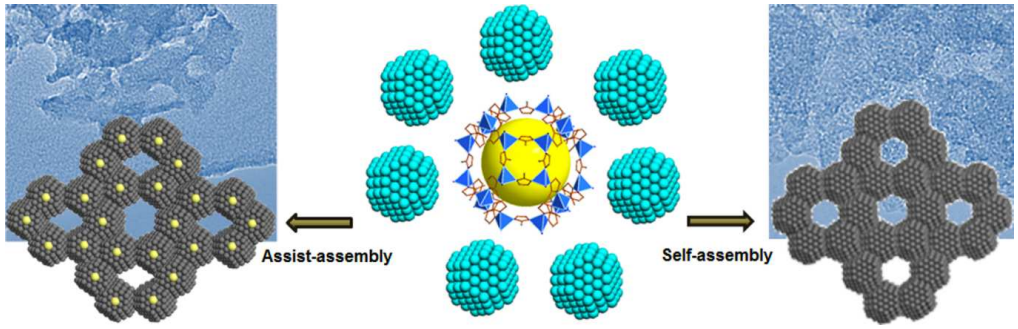

Creation of hierarchical pores is achieved by introducing self and extra porogenes in MOF-based porous carbons. In this strategy, the micropores and mesopores are inherited from well-ordered cavities of MOF crystals, and additional silica colloids with defined sizes. The bimodal porosities bring benefits to high storage capacitance and low charge-transport resistance, both of which make as-prepared nanoporous carbons as promising electrode materials in supercapacitors.